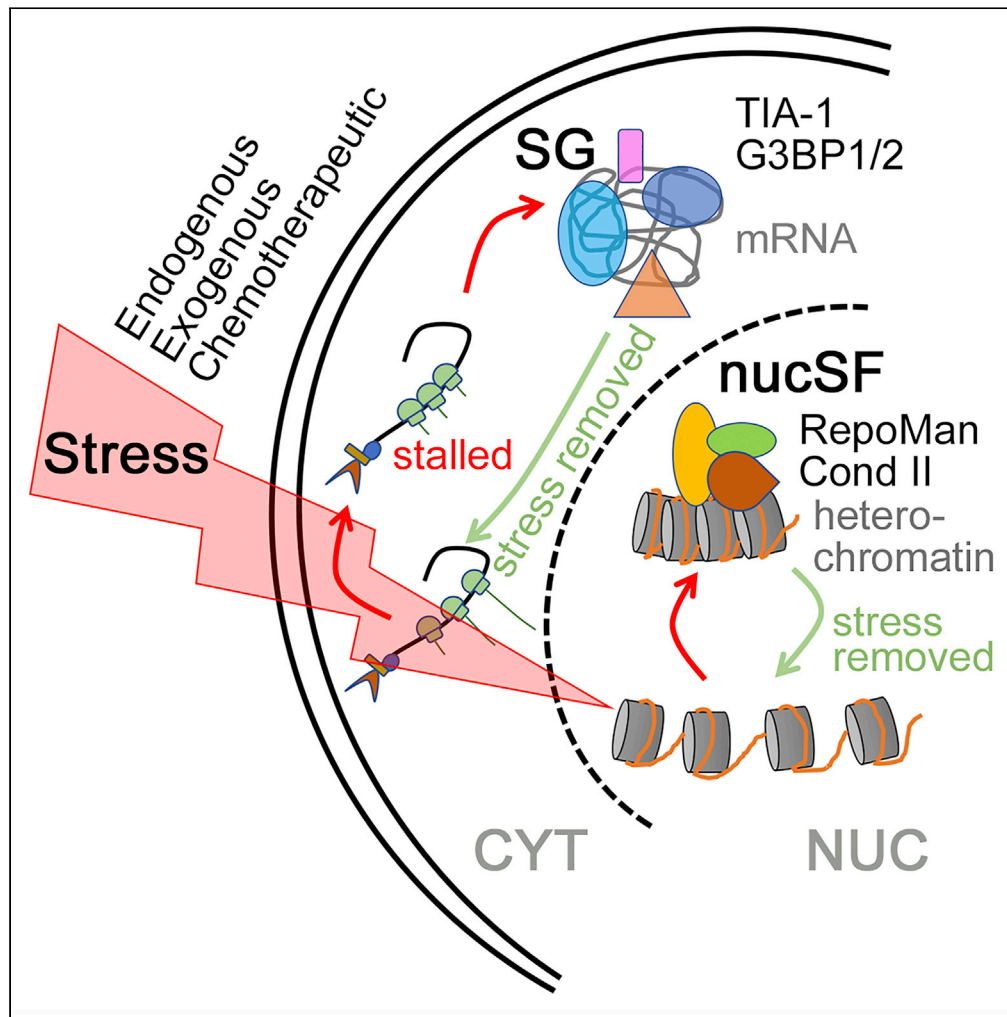


Article

# A Nuclear Stress Pathway that Parallels Cytoplasmic Stress Granule Formation



Tyler Quoc-Thai Do, Antoine Gaudreau-Lapierre, Carmen G. Pali, ..., Claire Simada Aeschmann, Majorie Brand, Laura Trinkle-Mulcahy

ltrinkle@uottawa.ca

**HIGHLIGHTS**

RepoMan and condensin II accumulate at nuclear foci in stressed cells

nucSF are triggered by stresses that induce canonical cytoplasmic stress granules

nucSF are sites of accumulation of heterochromatic markers

RepoMan shows increased association with the ADCY2 gene locus in arsenite-stressed cells

Do et al., iScience 23, 101664  
November 20, 2020 © 2020  
The Author(s).  
<https://doi.org/10.1016/j.isci.2020.101664>



## Article

A Nuclear Stress Pathway  
that Parallels Cytoplasmic Stress  
Granule Formation

Tyler Quoc-Thai Do,<sup>1,3</sup> Antoine Gaudreau-Lapierre,<sup>1,3</sup> Carmen G. Palii,<sup>2</sup> Virginia Maria Ferreira Resende,<sup>1</sup> Denise Campuzano,<sup>1</sup> Claire Simada Aeschmann,<sup>1</sup> Majorie Brand,<sup>2</sup> and Laura Trinkle-Mulcahy<sup>1,4,\*</sup>

## SUMMARY

**Stress adaptation is exploited by cancer cells to survive and proliferate under adverse conditions. Survival pathways induced by stress are thus highly promising therapeutic targets. One key pathway involves formation of cytoplasmic stress granules, which regulate the location, stability, and translation of specific mRNAs. Here, we describe a transcriptional stress response that is triggered by similar stressors and characterized by accumulation of RepoMan (cell division cycle associated 2) at nuclear stress foci (nucSF). Formation of these structures is reversible, and they are distinct from known nuclear organelles and stress bodies. Immunofluorescence analysis revealed accumulation of heterochromatic markers, and increased association of RepoMan with the adenylate cyclase 2 (ADCY2) gene locus in stressed cells accompanied reduced levels of ADCY2 mRNA and protein. Quantitative comparison of the RepoMan interactome in stressed vs. unstressed cells identified condensin II as a nucSF factor, suggesting their functional association in the establishment and/or maintenance of these facultative heterochromatic domains.**

## INTRODUCTION

In the face of adverse environmental conditions, cells activate an adaptive signaling pathway termed the integrated stress response (Pakos-Zebrucka et al., 2016). Stress-specific activation of one of four monitoring kinases (PERK, PKR, HRI, GCN2) that phosphorylate the eukaryotic translation initiation factor eIF2 $\alpha$  on Ser51 triggers cytoplasmic events that promote survival and restore cellular homeostasis. Phosphorylation shifts the balance of protein synthesis from active translation initiation to ribosomal runoff, and subsequent accumulation of stalled polysomes promotes formation of stress granules (SGs). These dynamic RNA/protein structures serve as triage sites that regulate the location, stability, and translation of specific mRNAs (Protter and Parker, 2016). A general reduction in global translation conserves energy and prevents accumulation of misfolded proteins, while selective translation of genes that promote cell survival and recovery is maintained (Lu et al., 2004). SGs also sequester key protein components, such as the TORC1 kinase that coordinates nutrient availability with cell growth (Takahara and Maeda, 2012). Upon removal of stress, eIF2 $\alpha$  is dephosphorylated, restoring normal protein synthesis and promoting SG disassembly (Lu et al., 2004). The microenvironment of solid tumors is often characterized by conditions that induce SG formation, such as low nutrient availability and a hypoxic core, and SG and SG-like foci have been detected in tumors of various origins. These include breast carcinoma and glioma (Baguet et al., 2007; Moeller et al., 2004; Somasekharan et al., 2015; Vilas-Boas et al., 2016). There is also increasing evidence that SGs, by contributing to re-programming of gene expression, promote tumor progression and development of therapeutic resistance (Anderson et al., 2015; Eisinger-Mathason et al., 2008; Grabocka and Bar-Sagi, 2016; Mahboubi and Stochaj, 2014; Somasekharan et al., 2015).

This study has uncovered a novel nuclear stress response that involves the rapid and reversible formation of heterochromatic domains in response to treatments that induce cytoplasmic SGs. Nuclear stress foci (nucSF) were first detected as an unexpected accumulation of the protein RepoMan within discrete nuclear foci in response to hypoxia. We originally identified RepoMan (cell division cycle associated 2 [Walker, 2001]) as a PP1 phosphatase regulatory subunit that recruits the catalytic subunit to chromatin-associated substrates (recruits PP1 onto mitotic chromatin at anaphase) (Trinkle-Mulcahy et al., 2006). Subsequent

<sup>1</sup>Department of Cellular and Molecular Medicine and Ottawa Institute of Systems Biology, Faculty of Medicine, University of Ottawa, Ottawa, ON K1H 8M5, Canada

<sup>2</sup>Sprott Center for Stem Cell Research, Ottawa Hospital Research Institute, Department of Cellular and Molecular Medicine, University of Ottawa, Ottawa, ON K1H 8L6, Canada

<sup>3</sup>These authors contributed equally

<sup>4</sup>Lead Contact

\*Correspondence:  
ltrinkle@uottawa.ca

<https://doi.org/10.1016/j.isci.2020.101664>



work linked the RepoMan/PP1 complex to regulation of key mitotic events that include chromosome segregation (Vagnarelli et al., 2006; Wurzenberger et al., 2012), chromosomal Aurora B kinase targeting (Qian et al., 2013, 2011), and nuclear envelope reassembly (Qian et al., 2011; Vagnarelli et al., 2011). Equally important non-mitotic roles were suggested by its persistence on chromatin during interphase and the cell cycle-independent apoptosis observed upon siRNA-mediated knockdown (Trinkle-Mulcahy et al., 2006). RepoMan/PP1 was shown to counteract the phosphorylation-mediated activation of ataxia-telangiectasia mutated, a key upstream signaling kinase in DNA damage response. As a consequence, excess RepoMan desensitizes cells to DNA damage (Peng et al., 2010), which can decrease genomic stability by allowing mutations to accumulate. Consistent with a pro-survival role, overexpression of RepoMan promotes proliferation of colorectal cancer and lung cancer adenocarcinoma cells in culture (Feng et al., 2019; Shi et al., 2017) while knockdown sensitizes oral squamous cell carcinoma cells to DNA damage-induced apoptosis (Uchida et al., 2013).

Increasing evidence points to RepoMan as a strong prognostic indicator that is elevated in numerous human cancers. RepoMan mRNA transcripts are overexpressed in late-stage cancers, with increased levels observed in breast, ovary, lung, and colon cancer tissues (Feng et al., 2019; Peng et al., 2010; Shi et al., 2017), as well as in oral squamous cell carcinoma and malignant breast cancer cell lines (Peng et al., 2010; Uchida et al., 2013; Vagnarelli, 2014). It is part of a cohort of 18 signature genes associated with malignant melanoma progression (Ryu et al., 2007) and one of two top-ranked genes correlated with metastatic behavior of synovial sarcomas (Lagarde et al., 2013). RepoMan is among the top scoring genes upregulated in aggressive stage 4 neuroblastoma tumors (Krasnoselsky et al., 2005), and high expression correlates with poor prognosis (Vagnarelli, 2014). RepoMan is also highly upregulated in tumor-infiltrating microglia in glioma-bearing brains (Giering et al., 2017), suggesting contribution to tumor immunity mechanisms that reprogram non-tumor cells within the tumor microenvironment.

More recently, RepoMan was shown to participate in heterochromatin formation in early G1, counteracting histone phosphorylation at mitotic exit to permit recruitment of heterochromatin proteins and accumulation of repressive histone marks (de Castro et al., 2017). We thus propose that nucSF represent facultative heterochromatin domains that function to repress specific genes as part of the cellular stress response. Association of RepoMan with these regions may explain its link to later stage cancers and poor prognosis and suggests that the nucSF pathway could be exploited to target cells that have developed therapeutic resistance through stress adaptation.

## RESULTS AND DISCUSSION

### Exogenous and Endogenous Cellular Stressors Induce Formation of nucSF in Parallel with Cytoplasmic SGs

Given that most solid tumors contain gradients of hypoxia and cells in hypoxic regions are the most aggressive and resistant to radiation and chemotherapy (Wilson and Hay, 2011), we were interested in testing whether or not excess RepoMan could further blunt the reduced DNA damage response observed in hypoxic cells. A surprising observation was that growth of cells in hypoxic conditions (1% O<sub>2</sub> for 24 hr) induced accumulation of RepoMan in multiple discrete nuclear foci (Figure 1A). These foci largely disassemble within 24 hr of re-oxygenation. Recruitment of RepoMan to nucSF requires its C-terminal half (Figure 1B), which governs association with chromatin (Prévost et al., 2013) (Vagnarelli et al., 2011). Fluorescence recovery after photobleaching (FRAP) experiments revealed a significantly reduced turnover rate for nucSF-associated green fluorescent protein (GFP)-tagged RepoMan, with no change in the overall mobile fraction (Figure 1C). We hypothesized that they may represent regions of more highly condensed chromatin. Senescence-associated heterochromatic foci induced by oncogenic stress and linked to suppression of pro-proliferative genes (Aird and Zhang, 2013; Narita et al., 2003) have been previously described; however, formation of nucSF (which are smaller and more numerous) is rapid and reversible, and cells continue to proliferate after recovery.

We screened a panel of 16 different cellular stressors that included DNA damaging agents, transcription and replication inhibitors, ER stress inducers, heat and osmotic shock, and nutrient starvation. Formation of nucSF was induced by a subset of stressors that, along with hypoxia, have also been shown to trigger formation of cytoplasmic SGs (Table S1; for review see (Mahboubi and Stochaj, 2017) (Protter and Parker, 2016)). These include sodium arsenite (Mahboubi et al., 2013), proteasome inhibition with MG132 (Mazroui et al., 2007) or the chemotherapeutic bortezomib (Fournier et al., 2010), osmotic stress (Dewey et al., 2011), heat shock (Mahboubi et al., 2013), and nutrient/serum starvation (Reineke et al., 2018). Of significance is

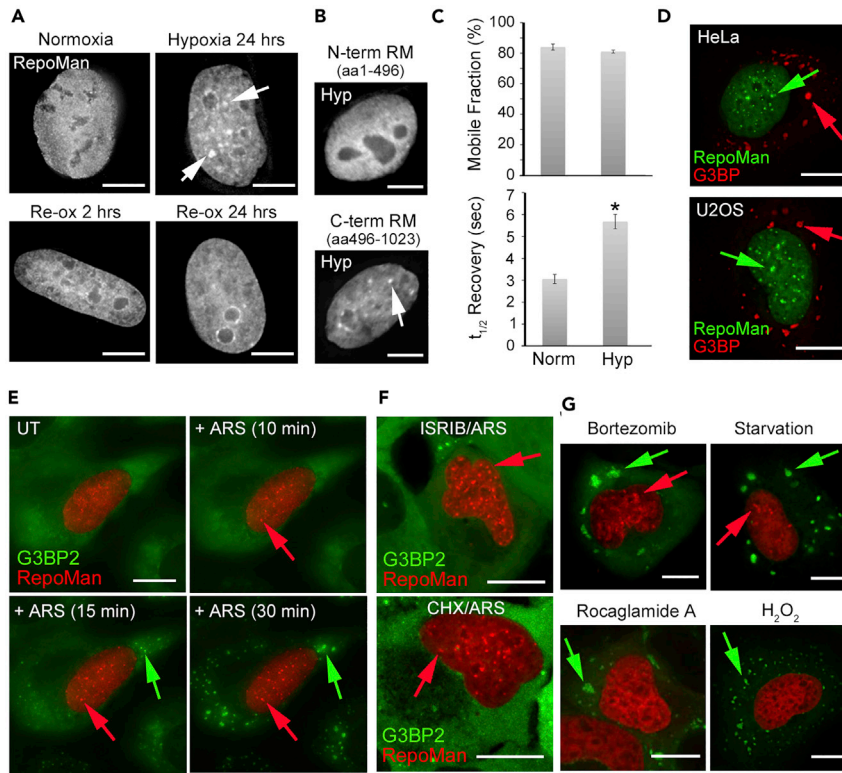


**Figure 1. Exogenous and Endogenous Stressors Trigger Formation of nucSF in Parallel with Cytoplasmic SGs**

(A) GFP-RepoMan transiently expressed in HeLa cells exposed to hypoxic (1% O<sub>2</sub>) conditions for 24 hr showed accumulation in multiple bright nuclear foci (arrows). These foci were largely resolved 24 hr after re-oxygenation (Re-ox). (B) Hypoxia (Hyp; 24 hr) triggered accumulation of the C-terminal half (aa 496–1023) but not the N-terminal half (aa 1–496) of RepoMan at nuclear foci (arrow). (C) FRAP analysis of GFP-RepoMan at hypoxia-induced nucSF revealed a significant decrease in turnover rate with no change in the overall mobile fraction (mean ± SE for >3 biological replicates; \*p = 2.3 × 10<sup>-6</sup> as determined by a paired Student's t-test). (D) GFP-RepoMan accumulates at nucSF (green arrows) in both HeLa and U2OS cells treated with 0.5 mM sodium arsenite for 30 min. The cells were fixed and stained with anti-G3BP to confirm formation of cytoplasmic SGs (red arrows). (E) Live imaging of U2OS cells stably expressing GFP-G3BP2 and transiently expressing mCherry-RepoMan. NucSF (red arrows) and SGs (green arrows) were detected as early as 10 and 15 min, respectively, following addition of 0.5 mM arsenite. See Video S1. (F) Inclusion of ISRIB (200 nM) or pre-treatment with CHX (50 μg/mL, 2 hr) selectively blocked SG but not nucSF formation in arsenite-treated cells. (G) Treatment with the proteasome inhibitor bortezomib (25 μM, 4 hr) and overnight glucose/serum starvation induced both SGs and nucSF, while treatment with the eIF4A inhibitor Rocaglamide (1 μM, 1 hr) or hydrogen peroxide (H<sub>2</sub>O<sub>2</sub>; 1 mM, 2 hr) selectively induced only SGs. See Video S2 for the full Rocaglamide A time course. Scale bars are 5 μm.

the fact that hypoxia, arsenite, and the proteasome inhibitor bortezomib have all been linked to promotion of therapy resistance (Fournier et al., 2010; Ganapathy et al., 2014; Wilson and Hay, 2011).

Figure 1D demonstrates formation of SGs and nucSF in HeLa and U2OS cells treated for 30 min with 0.5 mM arsenite. Arsenite-induced formation of SGs and nucSF was observed in additional cancer cell lines (MCF7, HCT116, SW480/620, SHSY5Y, NTERA-2), the virally transformed HEK293 cell line, and hTERT-immortalized retinal pigmented epithelial cells, suggesting that it is a conserved stress response (Table S2, Figure S2). Live imaging revealed that formation of arsenite-induced nucSF and SGs occurs on a similar timescale in U2OS cells (Figure 1E; Video S1).

Formation of SGs and nucSF in response to arsenite could be uncoupled by stressing cells in the presence of the small molecule integrated stress response inhibitor (ISRIB) (Figure 1F), which reverses the effects of

eIF2 $\alpha$  phosphorylation on translation and SG assembly (Sidrauski et al., 2015). Pre-treatment with cycloheximide, which stabilizes polysomes and prevents SG assembly (Kedersha et al., 2000), also selectively blocks SG but not nucSF formation (Figure 1F). Similarly, although the mechanism remains unclear, treatment with arsenite at a lower temperature inhibits SG formation (Wheeler et al., 2016), but does not affect nucSF formation (Figure S1N).

Stressors that induce SGs in a phospho-eIF2 $\alpha$ -independent manner did not induce nucSF (Figures 1G and S1). These include H<sub>2</sub>O<sub>2</sub>, which induces SGs that are compositionally distinct from canonical SGs and requires remodeling of the cap-binding eIF4E complex (Emara et al., 2012), and Rocaglamide A, which interferes with the RNA helicase eIF4A to induce formation of granules that are positive for core SG markers but negative for poly(A) mRNAs (Aulas et al., 2017) (Figure 1G; Video S2). Having observed that more extreme heat stress (45°C for 1 hr vs 30 min) was required to induce nucSF compared to SGs (Figures S1K–S1L), we extended the incubation time for Rocaglamide A from 1 to 6 hr but still did not see nucSF formation (Figure S1M). SG assembly can also be induced by overexpression of several SG-associated proteins, including TIA-1, which promotes nucleation and aggregation. In this case, nucSF assembly is not induced (Figures S1O–S1P). Taken together, these results suggest that the cellular and nuclear stress pathways are triggered by a shared kinase-mediated signaling event that is either upstream or related to activation of the eIF2 $\alpha$  stress kinases. This will be tested systematically in future work using a panel of inhibitors of various stress-related kinases.

It is also likely that nucSF, like SGs, have stress-specific properties. Although nucSF were induced by the osmotic stressors sorbitol and NaCl, for example, they were fewer in number and clustered at the nucleolar periphery (Figures S1I–S1J). NucSF induced by extreme heat shock showed this nucleolar clustering to an even greater extent (Figure S1L), which might represent a more dramatic reorganization of the chromatin landscape.

Importantly, heat shock- and arsenite-induced nucSF are distinct from the heat shock-induced nuclear stress bodies that accumulate mRNA processing factors and are marked by accumulation of heat shock factor 1 (Jolly et al., 1999; Figures S1L and S3H). And although RepoMan plays a role in DNA damage sensing, nucSF do not show accumulation of  $\gamma$ H2AX, which is a marker for sites of DNA double-strand breaks (Figure S3G [Mah et al., 2010]). NucSF are also distinct from previously described membraneless nuclear bodies that include promyelocytic leukemia protein (PML) bodies, Cajal bodies, splicing speckles, and paraspeckles (Figures S3A–S3D [Sleeman and Trinkle-Mulcahy, 2014]). These bodies are primarily enriched in RNA, whereas nucSF are sites of increased DNA but not RNA staining (Figures S1E–S1F). Chromatin insulator bodies are aggregates of chromatin insulator proteins that have been observed to form in response to osmotic stress in *Drosophila* nuclei (Schoborg et al., 2013). Their function is thought to be sequestration of insulator proteins away from DNA, with release triggered when cells are returned to isotonicity. Although they have not been observed in human cells, we stained arsenite-stressed cells with antibodies that recognized human CCCTC-binding factor (hCTCF), the human ortholog of *Drosophila* CTCF (dCTCF), to confirm that this factor does not show accumulation at nucSF (Figure S3I).

### nucSF Are Sites of Accumulation of Heterochromatic Markers

To determine whether nucSF represent regions of more highly condensed chromatin, we subjected arsenite-stressed cells to immunofluorescence analysis and confirmed accumulation of the heterochromatin markers HP1 $\gamma$  and tri-methylated lysine residue 9 of histone H3 (H3K9me3) at these regions (Figures 2A and 2B). Having noted partial overlap of the H3K9me3 and RepoMan signals (Figure 2B; see inset), we set out to define their spatial relationship at the nanoscale level using expansion microscopy (ExM)-based super-resolution imaging. ExM is a sample preparation technique in which fixed and stained cells are embedded in a dense cross-linked network of swellable polyelectrolyte hydrogel (Truckenbrodt et al., 2019). Addition of water isotropically expands the sample up to 10-fold, increasing the physical distance between biomolecules (Figure 2C). ExM was recently used to demonstrate functional subdomains in cytoplasmic SGs (Cirillo et al., 2020). Although structures can already be resolved at the sub-diffraction level (<200 nm) using a conventional microscope, we paired ExM (expansion factor calculated as  $\sim$ 7-fold; Figure S4A) with Airyscan imaging on an LSM880 confocal microscope to achieve a further 1.7x increase in resolution (Huff, 2015). We used ExM/Airyscan imaging and 3D volume rendering to demonstrate that H3K9me3 staining surrounds and spreads out from smaller RepoMan foci at nucSF (Figures 2D–2G). This suggests that RepoMan may play a role in nucSF nucleation and/or spreading and that individual nucSF may mediate repression of multiple genes.

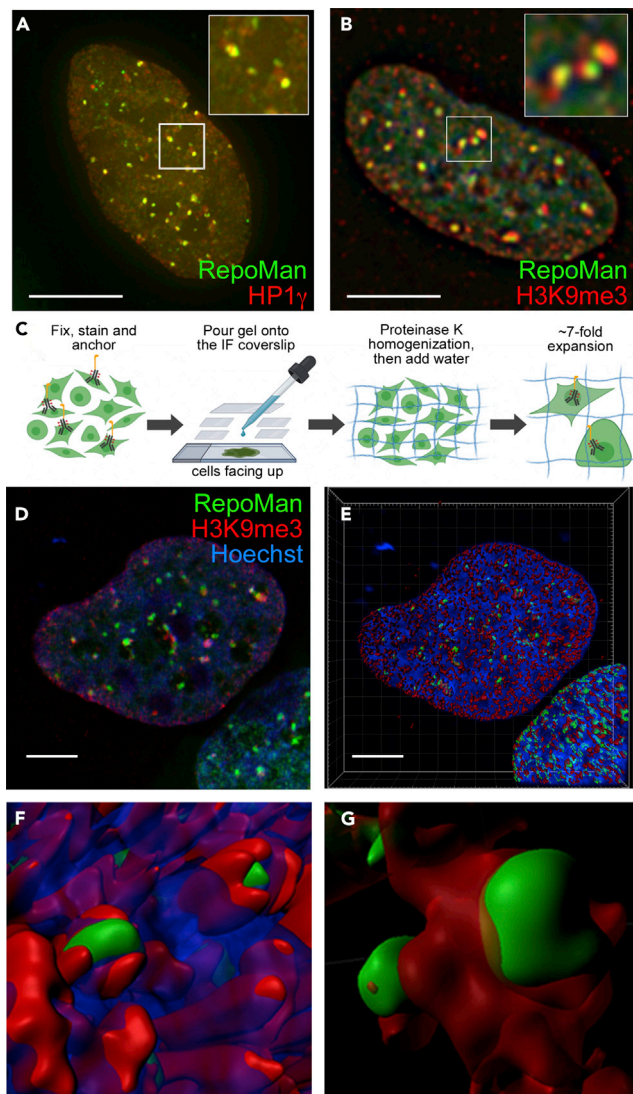


### Figure 2. NucSF are Sites of Accumulation of Heterochromatic Markers

(A and B) U2OS cells transiently expressing GFP-RepoMan (green) and treated with 0.5 mM arsenite for 30 min were fixed and stained with anti-HP1 $\gamma$  (A) or anti-H3K9me3 (B) and Alexa Fluor 555 secondary antibodies (red).

(C) Simplified model of ExM protocol. The expansion factor averaged 7.1x (see Figure S4).

(D) Airyscan image of an expanded arsenite-stressed U2OS cell expressing GFP-RepoMan and fixed and stained with anti-H3K9me3-AlexaFluor555 and Hoechst 33342.

(E) 3D volume rendering of the data set in (D).

(F and G) Enlarged insets (F and G) show RepoMan (green) relative to H3K9me3 (red) and DNA (blue). Scale bars are 5  $\mu$ m.

### Arsenite Induces Increased Association of RepoMan with the ADCY2 Gene Locus

Analysis of endogenous RepoMan has been limited by the lack of specific and reliable antibodies (de Castro et al., 2017; Prévost et al., 2013). We used CRISPR/Cas9 gene editing to fuse GFP to the N-terminus of endogenous RepoMan in HEK293 cells, confirming its shift in molecular mass by Western blot analysis and its expected subcellular localization by live imaging (Figures 3A and 3B). We also confirmed accumulation of endogenous GFP-tagged RepoMan at nucSF in response to arsenite treatment, using anti-TIA1 counter staining (Kedersha and Anderson, 2007) to mark SGs (Figure 3C). After 30 min of arsenite treatment, >90% of cells were positive for nucSF (>6 foci per cell; Figure 3D). These structures were fully disassembled 24 hr after removal of the stress.

We optimized GFP-RepoMan chromatin immunoprecipitation (ChIP) using this HEK293 knock-in cell line and confirmed association with two gene loci identified in a previously published *in vitro* screen to be bound by

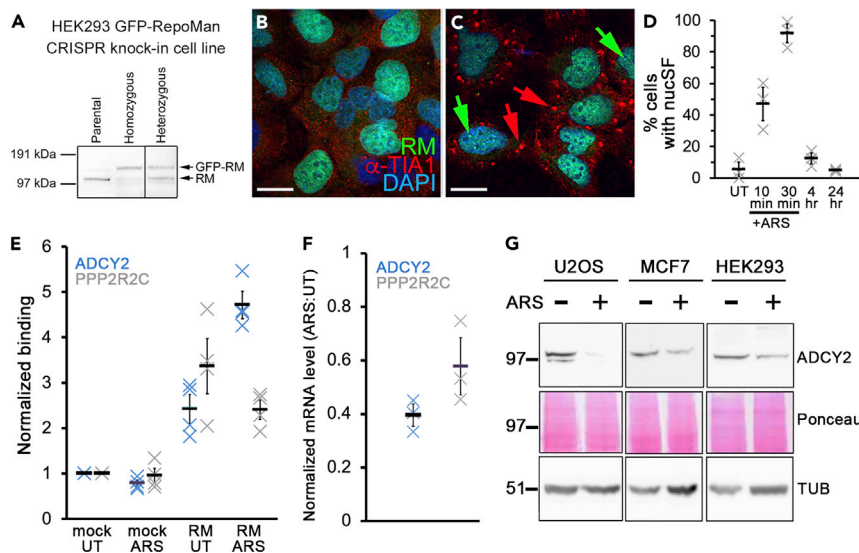


**Figure 3. Arsenite Stress Induces Increased Association of RepoMan with the ADCY2 Gene Locus**

(A) Western blot analysis of HEK293/GFP-RepoMan knock-in cell lysates with anti-RepoMan to assess the shift in molecular mass in heterozygous (single allele knock-in) and homozygous (double allele knock-in) cells. (B and C) To assess their response to acute arsenite treatment (0.5 mM for 30 min), homozygous cells were fixed following no treatment (B) or arsenite treatment (C) and stained with anti-TIA1 (red) and DAPI (blue). Green arrows indicate nucSF and red arrows point to SGs. Scale bars are 5  $\mu$ m. (D) Time course of arsenite-induced nucSF formation and disassembly in HEK293 GFP-RepoMan CRISPR knock-in cells. For each time point, multiple fields of view were imaged and cells scored for nucSF formation (>6 foci per cell). Results are shown for 3 independent experiments, with a total of 167–262 cells counted for each time point (mean  $\pm$  SE indicated by black bar). (E) ChIP-qPCR was used to compare binding of GFP-RepoMan to the ADCY2 (blue X) and PPP2R2C (gray X) gene loci in the knock-in cell line (untreated vs. 0.5 mM arsenite for 30 min). Mock immunoprecipitations (IPs) from untreated (UT) and arsenite-treated (ARS) lysates were included as controls, and all data normalized to the mock UT values. The experiment was repeated twice, with 2 technical replicates each time. Black bars indicate mean  $\pm$  standard deviation (SD). (F) RNA isolated from untreated vs. arsenite-stressed U2OS cells was subjected to RT-qPCR analysis. Values were normalized to GAPDH (see Figure S4 for confirmation that its cellular levels do not change with arsenite stress). Mean  $\pm$  standard error (SE) is indicated for 3 biological replicates. (G) Lysates from arsenite-stressed vs. untreated U2OS, MCF7, and HEK293 cells were subjected to Western blot analysis with anti-ADCY2.

Ponceau staining is shown for the corresponding region on the blot, and alpha-tubulin was stained as an additional loading control (TUB; see Figure S4 for confirmation that its cellular levels do not change with arsenite stress).

RepoMan: ADCY2 (adenylate cyclase) and PPP2R2C (PP2A regulatory subunit) (de Castro et al., 2017). ChIP-quantitative polymerase chain reaction (ChIP-qPCR) revealed increased association of RepoMan with the ADCY2 gene locus in response to arsenite treatment (Figure 3E), and reverse transcription PCR (RT-PCR) confirmed a >two-fold reduction in ADCY2 mRNA levels in arsenite-stressed cells (Figure 3F). Consistent with this, ADCY2 protein levels were shown by Western blot analysis to be reduced in arsenite-stressed U2OS, MCF7, and HEK293 cells (Figure 3G). Adenylate cyclase catalyzes production of cAMP from ATP. This second messenger plays a key role in regulation of cell proliferation, and upregulation of cAMP has been proposed as a cancer therapy approach (Chen et al., 1998; Fajardo et al., 2014; Li et al., 2016). Notably, adenylate cyclase was identified as one of the most highly downregulated proteins following long-term exposure of human embryonic carcinoma cells to low levels of arsenite (Das et al., 2011). Future experiments will utilize ChIP-sequencing (ChIP-seq) (Nakato and Sakata, 2020) and/or CUT&Tag (Kaya-Okur et al., 2019) approaches to identify additional nucSF target genes and determine whether, like SGs, there are stress-specific differences.

### Condensin II Accumulates at nucSF and Associates with RepoMan in Arsenite-Stressed Cells

To identify other factors that localize to nucSF, we compared the interactome of RepoMan in arsenite-stressed vs. untreated cells using two complementary strategies: (1) affinity purification/mass spectrometry (AP/MS), which identifies proteins that co-precipitate with affinity-purified bait protein, and (2) BioID, in which a biotin

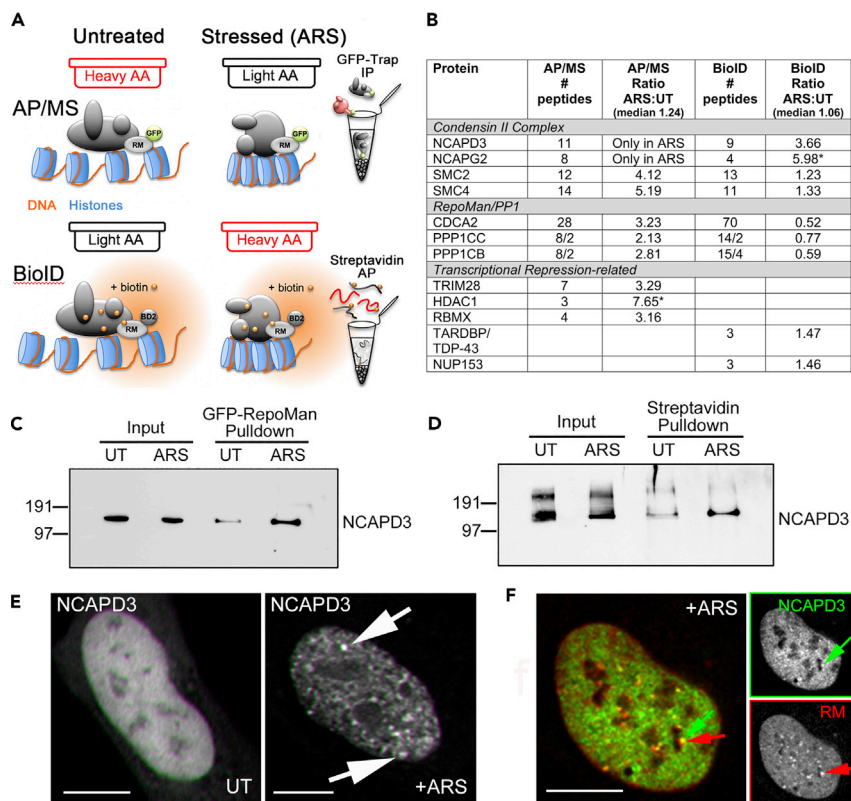


**Figure 4. Condensin II Accumulates at nucSF and Associates with RepoMan in Arsenite-Stressed Cells**

(A) Diagram detailing the complementary SILAC-based quantitative AP/MS and BioID strategies used to compare the interactome of RepoMan in arsenite-stressed vs untreated cells. For AP/MS, untreated cells were labeled with heavy (H) media and arsenite-treated cells with light (L) media. Endogenous GFP-tagged RepoMan in the HEK293 knock-in cell line was immunoprecipitated using the GFP-Trap\_A affinity resin and associated proteins identified by MS analysis. For BioID, the labeling strategy was flipped so that untreated cells were labeled with light media and arsenite-treated cells with heavy media. BioID2-tagged RepoMan was lentivirally transduced in U2OS cells and biotinylated proteins captured on streptavidin affinity resin and identified by MS analysis. ARS:UT ratios were determined for all proteins identified (L:H for AP/MS, (H)L for BioID).

(B) The table highlights overlapping and novel hits that showed increased association with RepoMan in single replicates of the internally controlled complementary screens (full data sets provided as Table S3). The number of peptides detected for each protein is listed, as well as its ratio ARS:UT (with the median ratio for the experiment listed for comparison). Note that in the AP/MS experiment NCAPD3 and NCAPG2 peptides were only detected in the L (+ARS) form. Asterisk (\*) indicates that MaxQuant did not calculate a SILAC ratio for the protein, so enrichment was estimated by comparing the summed L vs. H peptide intensities.

(C) AP/Western blot validation of the increased association of endogenous NCAPD3 with endogenous GFP-tagged RepoMan in arsenite-stressed HEK293 knock-in cells.

(D) BioID/Western blot validation of increased biotinylation of endogenous NCAPD3 by transduced BioID2-RepoMan in U2OS cells. Both blots were probed with anti-NCAPD3.

(E) Live imaging of U2OS cells stably expressing GFP-NCAPD3, either untreated (left panel) or treated with 0.5 mM arsenite for 30 min (arrows indicate stress-induced nuclear foci).

(F) Live imaging of U2OS cells stably expressing GFP-NCAPD3 (green) and transiently expressing mCherry-RepoMan (red), treated with 0.5 mM arsenite for 30 min to induce nucSF (red arrow) at which NCAPD3 (green arrow) accumulates. The inset panels show the individual NCAPD3 (top panel) and RepoMan (bottom panel) signals. Scale bars are 5 μm.

ligase fused to the bait protein drives biotinylation of proximal proteins for capture on a streptavidin affinity matrix and identification by MS (Figure 4A). Both incorporated SILAC (stable isotope labeling by amino acids [AAs] in culture) metabolic labeling to facilitate the robust and reliable identification of bona fide enriched factors above background contaminants (Trinkle-Mulcahy, 2012). The AP/MS experiment was performed using the GFP-RepoMan knock-in HEK293 cell line and high affinity GFP-Trap\_A resin (Trinkle-Mulcahy et al., 2008), with endogenous GFP-RepoMan captured from untreated cells labeled with heavy AAs and arsenite-stressed

cells (0.5 mM for 30 min) labeled with light AA. The BioID experiment was carried out in lentiviral-transduced U2OS cells expressing RepoMan fused to the smaller and more active BioID2 biotin ligase from *A. aeolicus* (Kim et al., 2016). The labeling strategy was reversed for this experiment, with biotin was added for 2 hr in the presence (heavy AA) or absence (light AA) of 0.1 mM arsenite. We also used a lower dose of arsenite for a longer incubation time to ensure efficient biotinylation and confirmed nucSF formation by staining fixed cells with fluorophore-tagged streptavidin (Figure S4D). Proteins that showed increased association with RepoMan in arsenite-stressed cells were readily identified by their increased light:heavy (AP/MS) or heavy:light (BioID) ratios (Table S3).

Overlapping hits, some of which are highlighted in the table in Figure 4B, include the condensin II complex members NCAPD3, NCAPG2, SMC2, and SMC4 (Uhlmann, 2016). In contrast to condensin I, condensin II is found in the nucleus throughout the cell cycle and has been proposed to play a role in establishment of chromatin architecture (Rosin et al., 2018). Increased association of NCAPD3 with RepoMan in arsenite-stressed cells was validated by AP/Western blot (Figure 4C) and BioID/Western blot (Figure 4D) analysis. We further confirmed recruitment of NCAPD3 to nucSF with arsenite treatment (Figure 4E), where it shows overlap with the RepoMan signal (Figure 4F). The subnuclear localization of NCAPD3 does not change in cells in which SGs are induced by TIA-1 overexpression (Figure S1P). Having previously shown that condensin II and the RepoMan/PP1 complex co-operate in the regulation of chromosome architecture during mitosis (Vagnarelli et al., 2006), we propose that they may also play a co-operative role in the regulation of nucSF formation and/or function in stressed cells. The observation of arsenite-induced NCAPD3 accumulation in nuclear foci in cells treated with RepoMan siRNA suggests that RepoMan may not be required for its recruitment to nucSF (Figure S4E); however, a more comprehensive analysis is required to determine whether these foci are functionally comparable to RepoMan-containing nucSF. RNAi-mediated RepoMan knockdown also triggers apoptotic pathways and widescale cell death that may confound the results (Trinkle-Mulcahy et al., 2006). Moving forward, we will take advantage of the temporal resolution of acute strategies such as auxin-inducible degradation (Li et al., 2019) to functionally dissect the contributions of RepoMan and NCAPD3 to this novel stress pathway.

With stress adaptation posing a significant challenge to the efficient treatment of cancer, characterization of cellular pro-survival pathways triggered by stress is essential for the identification of new molecular targets for both primary and adjuvant therapies. Factors involved in formation of cytoplasmic SGs are attractive candidates and have received significant attention recently. What these studies did not appreciate, however, is the nuclear stress pathway that we now know occurs in parallel with SG formation in response to similar endogenous and exogenous stressors. These findings thus open up an entirely new avenue of research.

### Limitations of the Study

Molecular dissection of the contributions of RepoMan and condensin II to the formation/function of nucSF is complicated by their key roles in other cellular pathways, such as cell cycle regulation and DNA damage response. This limits the usefulness of traditional knockdown/knockout approaches and necessitates optimization of more rapid protein depletion methods that can be implemented upstream of acute cellular stress.

### Resource Availability

#### Lead Contact

Further information and requests for resources and reagents should be directed to and will be fulfilled by the Lead Contact, Laura Trinkle-Mulcahy ([ltrinkle@uottawa.ca](mailto:ltrinkle@uottawa.ca)).

#### Materials Availability

All unique/stable reagents generated in this study are available from the Lead Contact with a completed Materials Transfer Agreement.

#### Data and Code Availability

The published article includes all data sets generated or analyzed during this study.

## METHODS

All methods can be found in the accompanying [Transparent Methods supplemental file](#).

## SUPPLEMENTAL INFORMATION

Supplemental Information can be found online at <https://doi.org/10.1016/j.isci.2020.101664>.

## ACKNOWLEDGMENTS

We thank colleagues in the Trinkle lab (Michèle Prévost, Jennifer Law, Sarah Ooi, and Virja Mehta) for their contributions and helpful discussions and Dr. Ryan Russell for advice and guidance with CRISPR/Cas9 gene editing. We also thank Lawrence Puente at the Ottawa Hospital Research Institute Proteomics Core Facility and Chloë van Oostende-Triplet and Skye Greene at the Cell Biology and Image Acquisition Core Facility for technical support. pSpCas9(BB)-2A-Puro (PX459) V2.0 was a gift from Feng Zhang (Addgene plasmid # 62988; <http://n2t.net/addgene:62988>; RRID:Addgene\_62988) and myc-BioID2-MCS was a gift from Kyle Roux (Addgene plasmid # 74223; <http://n2t.net/addgene:74223>; RRID:Addgene\_74223). This work was funded by the Cancer Research Society (20478) and Cancer Research Society/uOttawa Alliance (23484). T.D. was funded by a Natural Sciences and Engineering Research Council of Canada Undergraduate Student Research Award.

## AUTHOR CONTRIBUTIONS

T.D., A.G.L., and C.G.P. carried out methodology and investigation; D.C. carried out investigation and validation; C.S.A. and V.R. carried out investigation; M.B. provided methodology and resources; and L.T.M. was responsible for visualization, methodology, supervision, formal analysis, and writing.

## DECLARATION OF INTERESTS

The authors declare no competing interests.

Received: May 12, 2020

Revised: September 4, 2020

Accepted: October 7, 2020

Published: November 20, 2020

## REFERENCES

- Aird, K.M., and Zhang, R. (2013). Detection of senescence-associated heterochromatin foci (SAHF). In *Cell Senescence: Methods and Protocols*, Methods in Molecular Biology, L. Galluzzi, I. Vitale, O. Kepp, and G. Kroemer, eds. (Humana Press), pp. 185–196.
- Anderson, P., Kedersha, N., and Ivanov, P. (2015). Stress granules, P-bodies and cancer. *Biochim. Biophys. Acta* 1849, 861–870.
- Aulas, A., Fay, M.M., Lyons, S.M., Achorn, C.A., Kedersha, N., Anderson, P., and Ivanov, P. (2017). Stress-specific differences in assembly and composition of stress granules and related foci. *J. Cell Sci.* 130, 927–937.
- Baguet, A., Degot, S., Cougot, N., Bertrand, E., Chenard, M.-P., Wendling, C., Kessler, P., Hir, H.L., Rio, M.-C., and Tomasetto, C. (2007). The exon-junction-complex-component metastatic lymph node 51 functions in stress-granule assembly. *J. Cell Sci.* 120, 2774–2784.
- Chen, T.C., Hinton, D.R., Zidovetzki, R., and Hofman, F.M. (1998). Up-regulation of the cAMP/PKA pathway inhibits proliferation, induces differentiation, and leads to apoptosis in malignant gliomas. *Lab. Invest.* 78, 165–174.
- Cirillo, L., Cieren, A., Barbieri, S., Khong, A., Schwager, F., Parker, R., and Gotta, M. (2020). UBAP2L forms distinct cores that act in nucleating stress granules upstream of G3BP1. *Curr. Biol.* 30, 698–707.e6.
- Das, N.D., Park, J.H., Jung, K.H., Lee, H.T., Park, K.S., Choi, M.R., and Chai, Y.G. (2011). Sodium arsenite dependent protein expression analysis on human embryonic carcinoma (NCCIT) cell line. *Toxicol. Lett.* 207, 149–158.
- de Castro, I.J., Budzak, J., Di Giacinto, M.L., Ligamari, L., Gokhan, E., Spanos, C., Moralli, D., Richardson, C., de las Heras, J.I., Salatino, S., et al. (2017). Repo-Man/PP1 regulates heterochromatin formation in interphase. *Nat. Commun.* 8, 1–16.
- Dewey, C.M., Cenik, B., Sephton, C.F., Dries, D.R., Mayer, P., Good, S.K., Johnson, B.A., Herz, J., and Yu, G. (2011). TDP-43 is directed to stress granules by sorbitol, a novel physiological osmotic and oxidative stressor. *Mol. Cell. Biol.* 31, 1098–1108.
- Eisinger-Mathason, T.S.K., Andrade, J., Groehler, A.L., Clark, D.E., Muratore-Schroeder, T.L., Pasic, L., Smith, J.A., Shabanowitz, J., Hunt, D.F., Macara, I.G., and Lannigan, D.A. (2008). Codependent functions of RSK2 and the apoptosis-promoting factor TIA-1 in stress granule assembly and cell survival. *Mol. Cell* 31, 722–736.
- Emara, M.M., Fujimura, K., Sciaranghella, D., Ivanova, V., Ivanov, P., and Anderson, P. (2012). Hydrogen peroxide induces stress granule formation independent of eIF2 $\alpha$  phosphorylation. *Biochem. Biophys. Res. Commun.* 423, 763–769.
- Fajardo, A.M., Piazza, G.A., and Tinsley, H.N. (2014). The role of cyclic nucleotide signaling pathways in cancer: targets for prevention and treatment. *Cancers* 6, 436–458.
- Feng, Y., Qian, W., Zhang, Y., Peng, W., Li, J., Gu, Q., Ji, D., Zhang, Z., Wang, Q., Zhang, D., and Sun, Y. (2019). CDCA2 promotes the proliferation of colorectal cancer cells by activating the AKT/CCND1 pathway in vitro and in vivo. *BMC Cancer* 19, 576.
- Fournier, M.-J., Gareau, C., and Mazroui, R. (2010). The chemotherapeutic agent bortezomib induces the formation of stress granules. *Cancer Cell Int.* 10, 12.
- Ganapathy, S., Xiao, S., Seo, S.-J., Lall, R., Yang, M., Xu, T., Su, H., Shadfan, M., Ha, C.S., and Yuan, Z.-M. (2014). Low-dose arsenic induces chemotherapy protection via p53/NF- $\kappa$ B-mediated metabolic regulation. *Oncogene* 33, 1359–1366.
- Gieryng, A., Pszczolkowska, D., Bocian, K., Dabrowski, M., Rajan, W.D., Kloss, M., Mieczkowski, J., and Kaminska, B. (2017). Immune microenvironment of experimental rat C6 gliomas resembles human glioblastomas. *Sci. Rep.* 7, 1–14.
- Grabocka, E., and Bar-Sagi, D. (2016). Mutant KRAS enhances tumor cell fitness by upregulating stress granules. *Cell* 167, 1803–1813.e12.

- Huff, J. (2015). The Airyscan detector from ZEISS: confocal imaging with improved signal-to-noise ratio and super-resolution. *Nat. Methods* 12, i-ii.
- Jolly, C., Usson, Y., and Morimoto, R.I. (1999). Rapid and reversible relocalization of heat shock factor 1 within seconds to nuclear stress granules. *Proc. Natl. Acad. Sci. U S A* 96, 6769–6774.
- Kaya-Okur, H.S., Wu, S.J., Codomo, C.A., Pledger, E.S., Bryson, T.D., Henikoff, J.G., Ahmad, K., and Henikoff, S. (2019). CUT&Tag for efficient epigenomic profiling of small samples and single cells. *Nat. Commun.* 10, 1930.
- Kedersha, N., and Anderson, P. (2007). Mammalian stress granules and processing bodies. In *Methods in Enzymology, Translation Initiation: Cell Biology, High-Throughput Methods, and Chemical-Based Approaches* (Academic Press), pp. 61–81.
- Kedersha, N., Cho, M.R., Li, W., Yacono, P.W., Chen, S., Gilks, N., Golan, D.E., and Anderson, P. (2000). Dynamic shuttling of tia-1 accompanies the recruitment of mRNA to mammalian stress granules. *J. Cell Biol.* 151, 1257–1268.
- Kim, D.I., Jensen, S.C., Noble, K.A., Kc, B., Roux, K.H., Motamedchaboki, K., and Roux, K.J. (2016). An improved smaller biotin ligase for BiLD proximity labeling. *MBoC* 27, 1188–1196.
- Krasnoselsky, A.L., Whiteford, C.C., Wei, J.S., Bilke, S., Westermann, F., Chen, Q.-R., and Khan, J. (2005). Altered expression of cell cycle genes distinguishes aggressive neuroblastoma. *Oncogene* 24, 1533–1541.
- Lagarde, P., Przybyl, J., Brulard, C., Pérot, G., Pierron, G., Delattre, O., Sciot, R., Wozniak, A., Schöffski, P., Terrier, P., et al. (2013). Chromosome instability accounts for reverse metastatic outcomes of pediatric and adult synovial sarcomas. *JCO* 31, 608–615.
- Li, K., Zhang, H., Qiu, J., Lin, Y., Liang, J., Xiao, X., Fu, L., Wang, F., Cai, J., Tan, Y., et al. (2016). Activation of cyclic adenosine monophosphate pathway increases the sensitivity of cancer cells to the oncolytic virus M1. *Mol. Ther.* 24, 156–165.
- Li, S., Prasanna, X., Salo, V.T., Vattulainen, I., and Ikonen, E. (2019). An efficient auxin-inducible degron system with low basal degradation in human cells. *Nat. Methods* 16, 866–869.
- Lu, P.D., Harding, H.P., and Ron, D. (2004). Translation reinitiation at alternative open reading frames regulates gene expression in an integrated stress response. *J. Cell Biol.* 167, 27–33.
- Mah, L.-J., El-Osta, A., and Karagiannis, T.C. (2010).  $\gamma$ H2AX: a sensitive molecular marker of DNA damage and repair. *Leukemia* 24, 679–686.
- Mahboubi, H., Kodiaha, M., and Stochaj, U. (2013). Automated detection and quantification of granular cell compartments. *Microsc. Microanal.* 19, 617–628.
- Mahboubi, H., and Stochaj, U. (2017). Cytoplasmic stress granules: dynamic modulators of cell signaling and disease. *Biochim. Biophys. Acta* 1863, 884–895.
- Mahboubi, H., and Stochaj, U. (2014). Nucleoli and stress granules: connecting distant relatives. *Traffic* 15, 1179–1193.
- Mazroui, R., Di Marco, S., Kaufman, R.J., and Gallouzi, I.-E. (2007). Inhibition of the ubiquitin-proteasome system induces stress granule formation. *MBoC* 18, 2603–2618.
- Moeller, B.J., Cao, Y., Li, C.Y., and Dewhirst, M.W. (2004). Radiation activates HIF-1 to regulate vascular radiosensitivity in tumors: role of reoxygenation, free radicals, and stress granules. *Cancer Cell* 5, 429–441.
- Nakato, R., and Sakata, T. (2020). Methods for ChIP-seq analysis: a practical workflow and advanced applications. *Methods* S1046-2023, S1046-2023(20)30059-1.
- Narita, Masashi, Nuñez, S., Heard, E., Narita, Masako, Lin, A.W., Hearn, S.A., Spector, D.L., Hannon, G.J., and Lowe, S.W. (2003). Rb-mediated heterochromatin formation and silencing of E2F target genes during cellular senescence. *Cell* 113, 703–716.
- Pakos-Zebrucka, K., Koryga, I., Mnich, K., Ljujic, M., Samali, A., and Gorman, A.M. (2016). The integrated stress response. *EMBO Rep.* 17, 1374–1395.
- Peng, A., Lewellyn, A.L., Schiemann, W.P., and Maller, J.L. (2010). Repo-man controls a protein phosphatase 1-dependent threshold for DNA damage checkpoint activation. *Curr. Biol.* 20, 387–396.
- Prévost, M., Chamoussat, D., Nasa, I., Freele, E., Morrice, N., Moorhead, G., and Trinkle-Mulcahy, L. (2013). Quantitative fragmentome mapping reveals novel, domain-specific partners for the modular protein RepoMan (recruits PP1 onto mitotic chromatin at anaphase). *Mol. Cell Proteomics* 12, 1468–1486.
- Protter, D.S.W., and Parker, R. (2016). Principles and properties of stress granules. *Trends Cell Biol.* 26, 668–679.
- Qian, J., Beullens, M., Lesage, B., and Bollen, M. (2013). Aurora B defines its own chromosomal targeting by opposing the recruitment of the phosphatase scaffold repo-man. *Curr. Biol.* 23, 1136–1143.
- Qian, J., Lesage, B., Beullens, M., Van Eynde, A., and Bollen, M. (2011). PP1/Repo-Man dephosphorylates mitotic histone H3 at T3 and regulates chromosomal Aurora B targeting. *Curr. Biol.* 21, 766–773.
- Reineke, L.C., Cheema, S.A., Dubrulle, J., and Neilson, J.R. (2018). Chronic starvation induces noncanonical pro-death stress granules. *J. Cell Sci.* 131, jcs220244.
- Rosin, L.F., Nguyen, S.C., and Joyce, E.F. (2018). Condensin II drives large-scale folding and spatial partitioning of interphase chromosomes in *Drosophila* nuclei. *PLoS Genet.* 14, e1007393.
- Ryu, B., Kim, D.S., Deluca, A.M., and Alani, R.M. (2007). Comprehensive expression profiling of tumor cell lines identifies molecular signatures of melanoma progression. *PLoS One* 2, e594.
- Schoborg, T., Rickels, R., Barrios, J., and Labrador, M. (2013). Chromatin insulator bodies are nuclear structures that form in response to osmotic stress and cell death. *J. Cell Biol.* 202, 261–276.
- Shi, R., Zhang, C., Wu, Y., Wang, X., Sun, Q., Sun, J., Xia, W., Dong, G., Wang, A., Jiang, F., and Xu, L. (2017). CDCA2 promotes lung adenocarcinoma cell proliferation and predicts poor survival in lung adenocarcinoma patients. *Oncotarget* 8, 19768–19779.
- Sidrauski, C., McGeachy, A.M., Ingolia, N.T., and Walter, P. (2015). The small molecule ISRIB reverses the effects of eIF2 $\alpha$  phosphorylation on translation and stress granule assembly. *Elife* 4, e05033.
- Sleeman, J.E., and Trinkle-Mulcahy, L. (2014). Nuclear bodies: new insights into assembly/dynamics and disease relevance. *Curr. Opin. Cell Biol.* 28, 76–83.
- Somasekharan, S.P., El-Naggar, A., Leprivier, G., Cheng, H., Hajee, S., Grunewald, T.G.P., Zhang, F., Ng, T., Delattre, O., Evdokimova, V., et al. (2015). YB-1 regulates stress granule formation and tumor progression by translationally activating G3BP1. *J. Cell Biol.* 208, 913–929.
- Takahara, T., and Maeda, T. (2012). Transient sequestration of TORC1 into stress granules during heat stress. *Mol. Cell* 47, 242–252.
- Trinkle-Mulcahy, L. (2012). Resolving protein interactions and complexes by affinity purification followed by label-based quantitative mass spectrometry. *Proteomics* 12, 1623–1638.
- Trinkle-Mulcahy, L., Andersen, J., Lam, Y.W., Moorhead, G., Mann, M., and Lamond, A.I. (2006). Repo-Man recruits PP1 gamma to chromatin and is essential for cell viability. *J. Cell Biol.* 172, 679–692.
- Trinkle-Mulcahy, L., Boulon, S., Lam, Y.W., Urcia, R., Boisvert, F.-M., Vandermoere, F., Morrice, N.A., Swift, S., Rothbauer, U., Leonhardt, H., and Lamond, A. (2008). Identifying specific protein interaction partners using quantitative mass spectrometry and bead proteomes. *J. Cell Biol.* 183, 223–239.
- Truckenbrodt, S., Sommer, C., Rizzoli, S.O., and Danzl, J.G. (2019). A practical guide to optimization in X10 expansion microscopy. *Nat. Protoc.* 14, 832–863.
- Uchida, F., Uzawa, K., Kasamatsu, A., Takatori, H., Sakamoto, Y., Ogawara, K., Shiiba, M., Bukawa, H., and Tanzawa, H. (2013). Overexpression of CDCA2 in human squamous cell carcinoma: correlation with prevention of G1 phase Arrest and apoptosis. *PLoS One* 8, e56381.
- Uhlmann, F. (2016). SMC complexes: from DNA to chromosomes. *Nat. Rev. Mol. Cell Biol.* 17, 399–412.
- Vagnarelli, P. (2014). Repo-Man at the intersection of chromatin remodelling, DNA repair, nuclear envelope organization, and cancer progression. In *Cancer Biology and the Nuclear Envelope: Recent Advances May Elucidate Past Paradoxes, Advances in Experimental Medicine and Biology*, E.C. Schirmer and J.I. de las Heras, eds. (Springer), pp. 401–414.
- Vagnarelli, P., Hudson, D.F., Ribeiro, S.A., Trinkle-Mulcahy, L., Spence, J.M., Lai, F., Farr, C.J.,

Lamond, A.I., and Earnshaw, W.C. (2006). Condensin and Repo-Man-PP1 co-operate in the regulation of chromosome architecture during mitosis. *Nat. Cell Biol.* 8, 1133–1142.

Vagnarelli, P., Ribeiro, S., Sennels, L., Sanchez-Pulido, L., de Lima Alves, F., Verheyen, T., Kelly, D.A., Ponting, C.P., Rappsilber, J., and Earnshaw, W.C. (2011). Repo-Man coordinates chromosomal reorganization with nuclear envelope reassembly during mitotic exit. *Dev. Cell* 21, 328–342.

Vilas-Boas, F.de A.S., da Silva, A.M., de Sousa, L.P., Lima, K.M., Vago, J.P., Bittencourt, L.F.F., Dantas, A.E., Gomes, D.A., Vilela, M.C., Teixeira, M.M., and Barcelos, L.S. (2016). Impairment of stress granule assembly via inhibition of the eIF2alpha phosphorylation sensitizes glioma cells to chemotherapeutic agents. *J. Neurooncol.* 127, 253–260.

Walker, M.G. (2001). Drug target discovery by gene expression analysis cell cycle genes. *Curr. Cancer Drug Targets* 1, 73–83.

Wheeler, J.R., Matheny, T., Jain, S., Abrisch, R., and Parker, R. (2016). Distinct stages in stress granule assembly and disassembly. *Elife* 5, e18413.

Wilson, W.R., and Hay, M.P. (2011). Targeting hypoxia in cancer therapy. *Nat. Rev. Cancer* 11, 393–410.

Wurzenberger, C., Held, M., Lampson, M.A., Poser, I., Hyman, A.A., and Gerlich, D.W. (2012). Sds22 and Repo-Man stabilize chromosome segregation by counteracting Aurora B on anaphase kinetochores. *J. Cell Biol.* 198, 173–183.

**iScience, Volume 23**

## **Supplemental Information**

### **A Nuclear Stress Pathway that Parallels Cytoplasmic Stress Granule Formation**

**Tyler Quoc-Thai Do, Antoine Gaudreau-Lapierre, Carmen G. Pali, Virginia Maria Ferreira Resende, Denise Campuzano, Claire Simada Aeschmann, Majorie Brand, and Laura Trinkle-Mulcahy**

## Supplemental Tables

Stress	Mode of Action	nucSF/SG Formation
Sodium Arsenite (0.5 mM, 30 min)	ROS production	Yes/Yes (Fig. 1d)
Bortezomib (25 $\mu$ M, 4 hrs)	Inhibits 26S Proteasome	Yes/Yes (Fig. 1g)
Serum/glucose-free media (overnight)	Nutrient/serum starvation	Yes/Yes (Fig. 1g)
Rocaglamide A (1 $\mu$ M, 1 hr)	Inhibits eIF4A	No/Yes* (Fig. 1g)
Rocaglamide A (1 $\mu$ M, 6 hr)	Inhibits eIF4A	No/Yes* (Fig. S1m)
Hydrogen peroxide (1 mM, 2 hrs)	Oxidative stress	No/Yes* (Fig. 1g)
Actinomycin D (2.5 $\mu$ g/ml, 2 hrs)	Inhibits RNA transcription	No/No (Fig. S1a)
5,6-Dichlorobenzimidazole 1- $\beta$ -D-ribofuranoside (DRB; 25 $\mu$ g/ml, 2 hrs)	Inhibits CTD kinases	No/No (Fig. S1b)
Hydroxyurea (2 mM, overnight)	Inhibits DNA synthesis	No/No (Fig. S1c)
Camptothecin (1 $\mu$ g/ml, 1 hr)	Inhibits DNA topoisomerase I	No/No (Fig. S1d)
Cisplatin (1 $\mu$ g/ml, overnight)	Crosslinks DNA	No/No (Fig. S1e)
Etoposide (50 $\mu$ M, 4 hrs)	Inhibits DNA Topoisomerase II	No/No (Fig. S1f)
Olaparib (10 $\mu$ M, overnight)	Inhibits PARP	No/No (Fig. S1g)
MG132 (10 $\mu$ g/ml, 1 hr)	Inhibits 26S proteasome	Yes/Yes (Fig. S1h)
Sorbitol (0.4 M, 1 hr)	Osmotic stress	Yes <sup>^</sup> /Yes* (Fig. S1i)
NaCl (0.2 M, 1 hr)	Osmotic stress	Yes <sup>^</sup> /Yes* (Fig. S1j)
Heat Shock (45°C, 30 min)	Heat stress	No/Yes (Fig. S1k)
Heat Shock (45°C, 1 hr)	Heat stress (extreme)	Yes <sup>^</sup> /Yes (Fig. S1l)
TIA-1 overexpression	Aggregation of SG factors	No/Yes* (Fig. S1o-p)

**Table S1. Summary of cellular stresses tested for nucSF and SG formation, Related to Figures 1 and S1.** Formation of nucSF and cytoplasmic SGs was assessed in U2OS cells (see indicated panels in Figures 1 and S1). Yes = >50% of cells have >6 nuclear foci and/or SGs. \*non-canonical SGs. <sup>^</sup> fewer nuclear foci, clustered at the nucleolar periphery.

Cell Line	Description	nucSF/SG formation
HeLa	Cervical carcinoma (f)	Yes/Yes (Fig. 1d)
U-2 OS	Osteosarcoma (f)	Yes/Yes (Fig. 1d)
MCF7	Breast cancer, derived from metastatic site (f)	Yes/Yes (Fig. S1a)
NTERA-2	Pluripotent testicular embryonal carcinoma (m)	Yes/Yes (Fig. S2b)
SH-SY5Y	Neuroblastoma (f)	Yes/Yes (Fig. S2c)
HCT116	Colorectal carcinoma (m)	Yes/Yes (Fig. S2d)
SW480	Colorectal adenocarcinoma (m)	Yes/Yes (Fig. S2e)
SW620	Colorectal adenocarcinoma, derived from metastatic site (m)	Yes/Yes (Fig. S2f)
HEK293	Embryonic kidney, adenoviral-transformed (f)	Yes/Yes (Fig. S2g)
RPE-1	Retinal pigmented epithelium, hTERT-immortalized (f)	Yes/Yes (Fig. S2h)

**Table S2. Summary of cultured human cell lines tested for arsenite-induced nucSF and SG formation, Related to Figure 1 and S2.** Cells transiently expressing GFP-RepoMan were treated with arsenite (0.5 mM, 30 min), fixed and stained with anti-G3BP to assess formation of nucSF and SGs (see indicated panels in Figures 1 and S2). Yes = >50% of cells had >6 nuclear foci and/or SGs. (f) = female. (m) = male.

Supplemental Figures

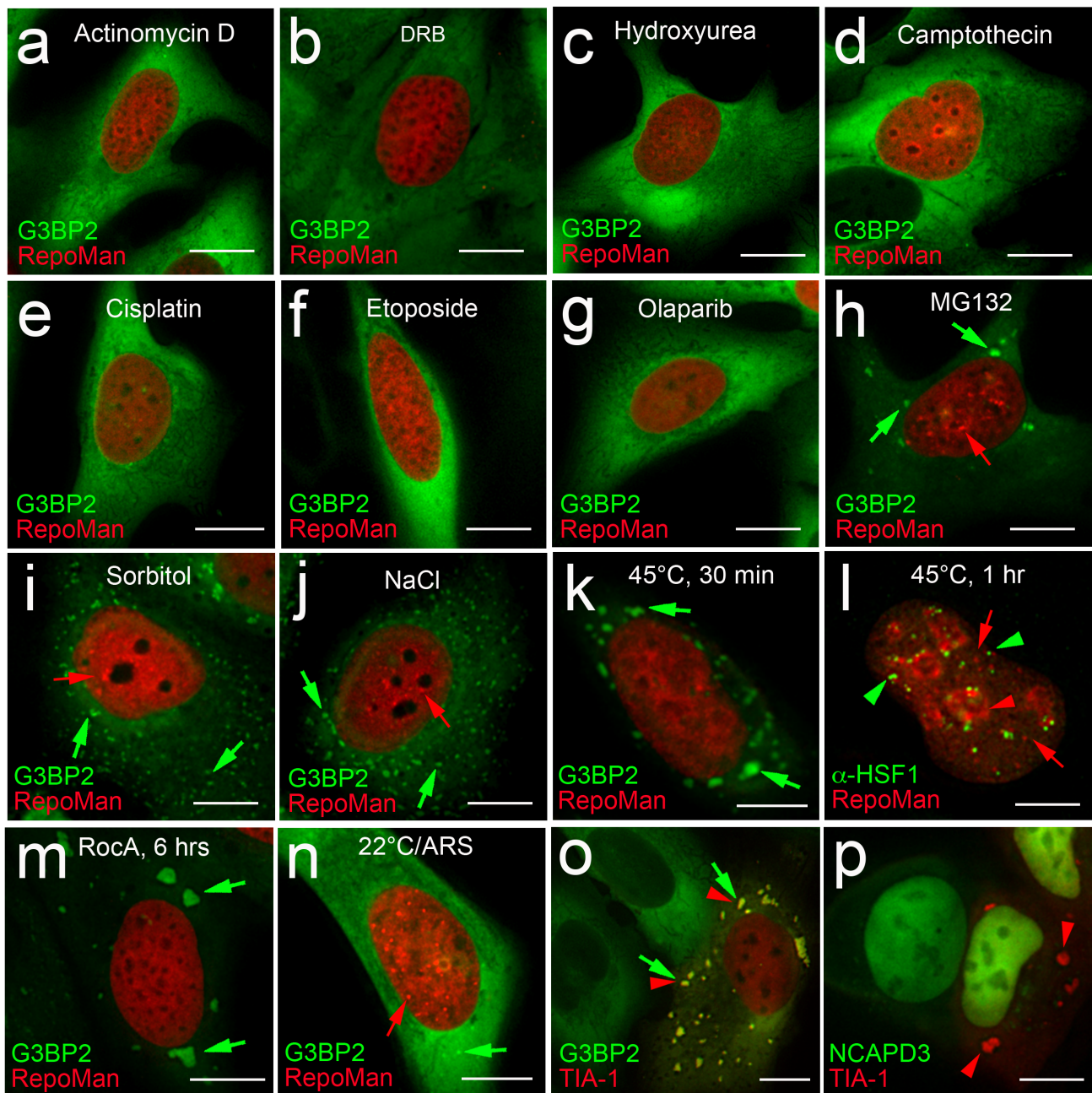


**Figure S1. Stress-specific formation of nucSF and cytoplasmic SGs, Related to Figure 1.** a-k, m-n. U2OS cells stably expressing GFP-G3BP2 (green) and transiently expressing mCh-RepoMan (red) were subjected to the treatment indicated at the top of each panel and imaged live to assess formation of nucSF (red arrows) and SGs (green arrows). See Table S2 for details of each treatment (concentration, time, mode of action). Cells exposed to heat shock were fixed prior to imaging (k-l). In response to more extreme heat shock (45°C for 1 hr), accumulation of mCh-RepoMan at small nucSF (red arrows) and the peri-nucleolar region (red arrowhead) in parental U2OS cells was observed (l). For this experiment, the cells were fixed and stained with anti-HSF1 (green) to mark heat shock-induced nuclear stress bodies (green arrowheads). o. Transient overexpression of mCh-TIA1 in U2OS cells stably expressing G3BP2 induced SGs containing both proteins (red arrowheads, green arrows) but did not trigger accumulation of NCAPD3 in nucSF (p). Scale bars are 5 μm.

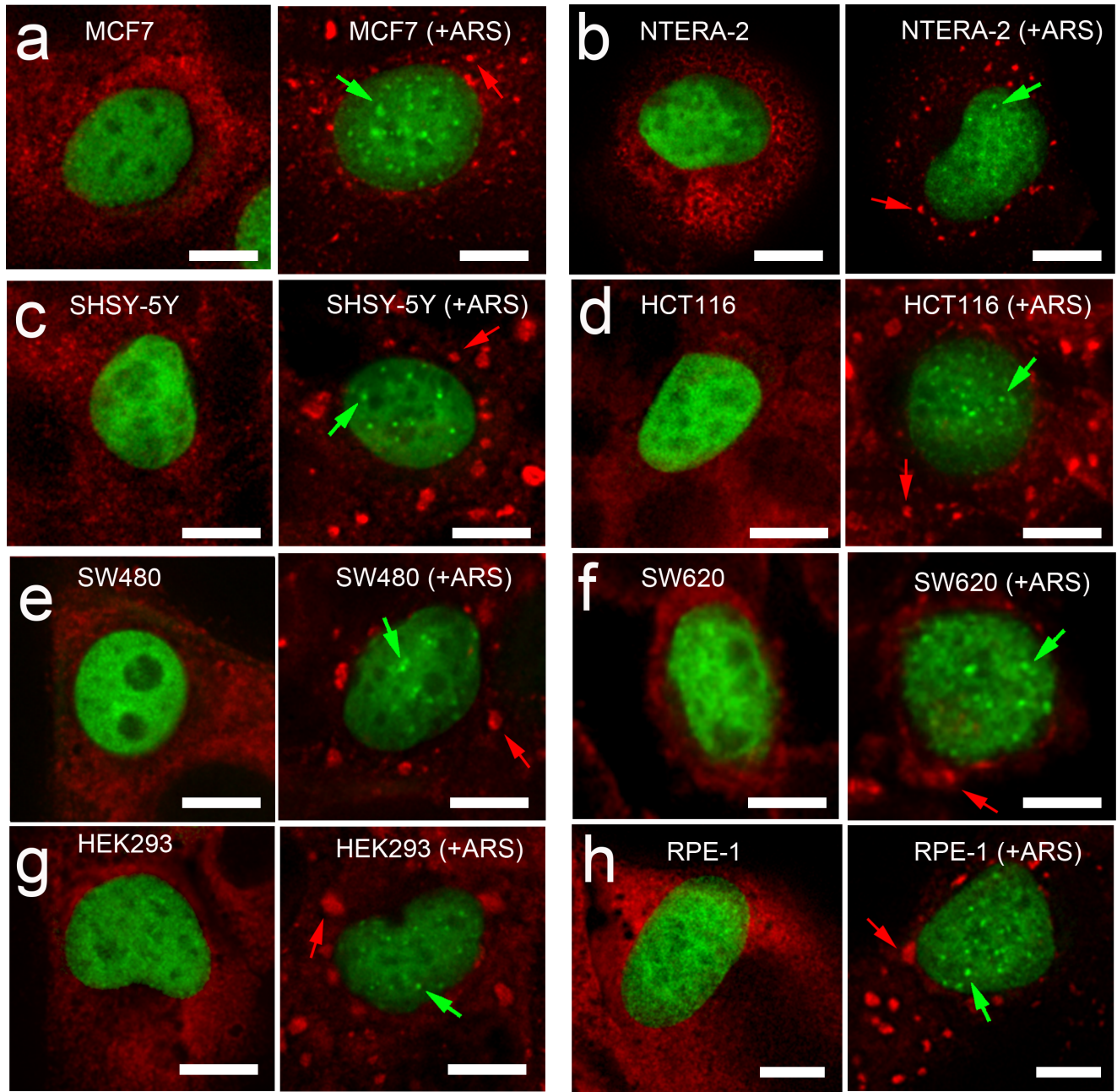


**Figure S2. Arsenite stress induces formation of nucSF and cytoplasmic SGs in a range of cultured cell lines, Related to Figure 1.** a-h. The cell lines indicated at the top of each panel were transiently transfected with GFP-RepoMan and either left untreated or treated with 0.5 mM arsenite for 30 min prior to fixation (+ARS). The fixed cells were stained with anti-G3BP (red). Green arrows point to nucSF while red arrows point to SGs. Scale bars are 5  $\mu$ m.

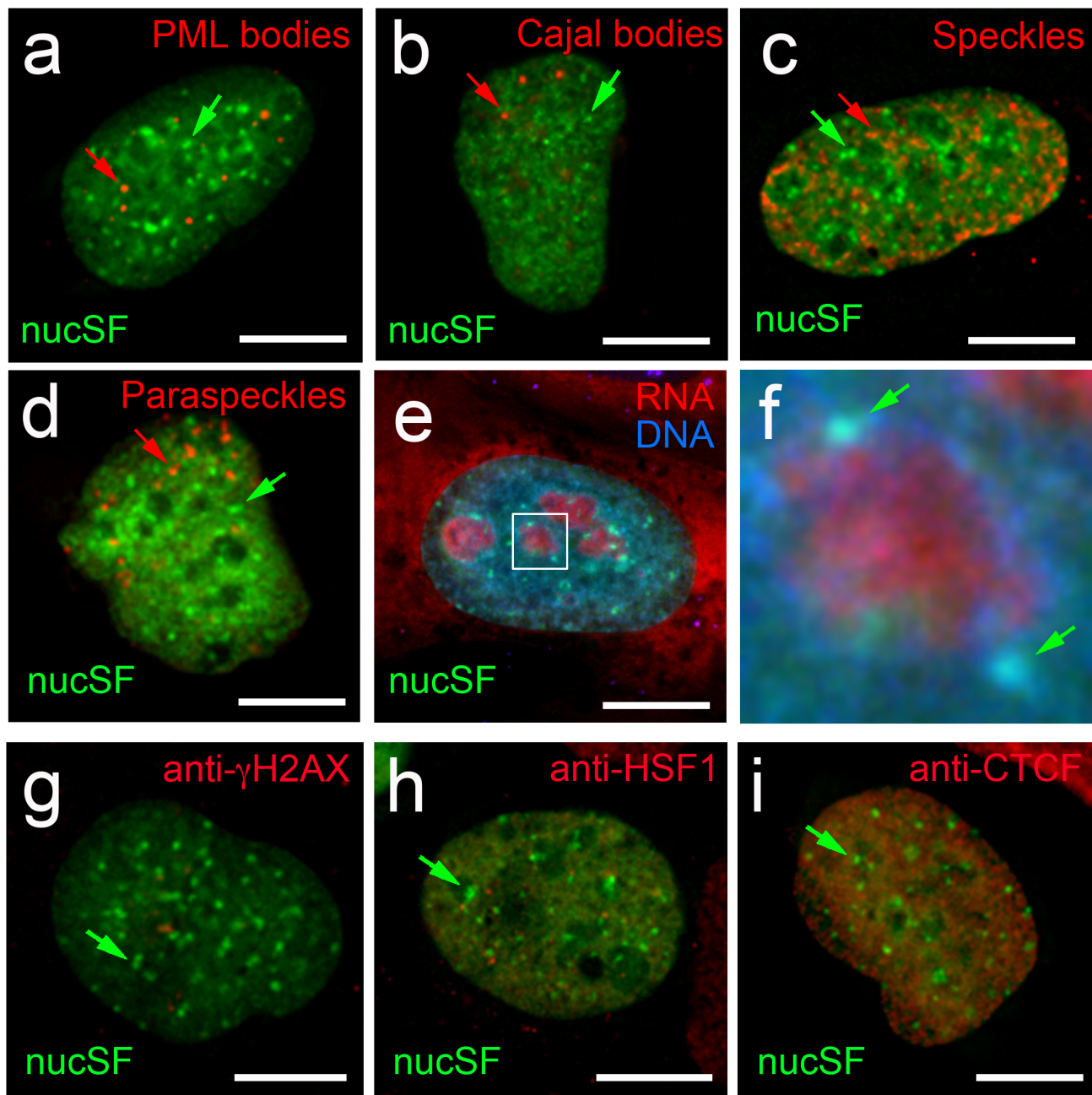


**Figure S3. Arsenite-induced nucSF marked by accumulation of GFP-RepoMan in U2OS cells are distinct from other known nuclear bodies, Related to Figure 2.** No overlap is detected between nucSF (GFP-RepoMan; green arrows) and nuclear organelles such as PML bodies (a; anti-PML; red arrows), Cajal bodies (b; anti-Coilin; red arrows), splicing speckles (c; anti-Y12; red arrows) or paraspeckles (d; mCh-PSP1; red arrows). Increased Hoechst 33342 (DNA; blue) but not Pyronin Y (RNA; red) staining is observed in nucSF (e; f is expanded view of the region delineated by the white box). The arsenite treatment used (0.5 mM for 30 min) did not induce accumulation of either  $\gamma$ H2AX (g; marker for sites of double-strand DNA breaks) or HSF1 (h; marker for heat shock-induced nuclear stress bodies). i. No localized accumulation of the chromatin insulator factor CTCF was observed in arsenite-stressed cells. Scale bars are 5  $\mu$ m.

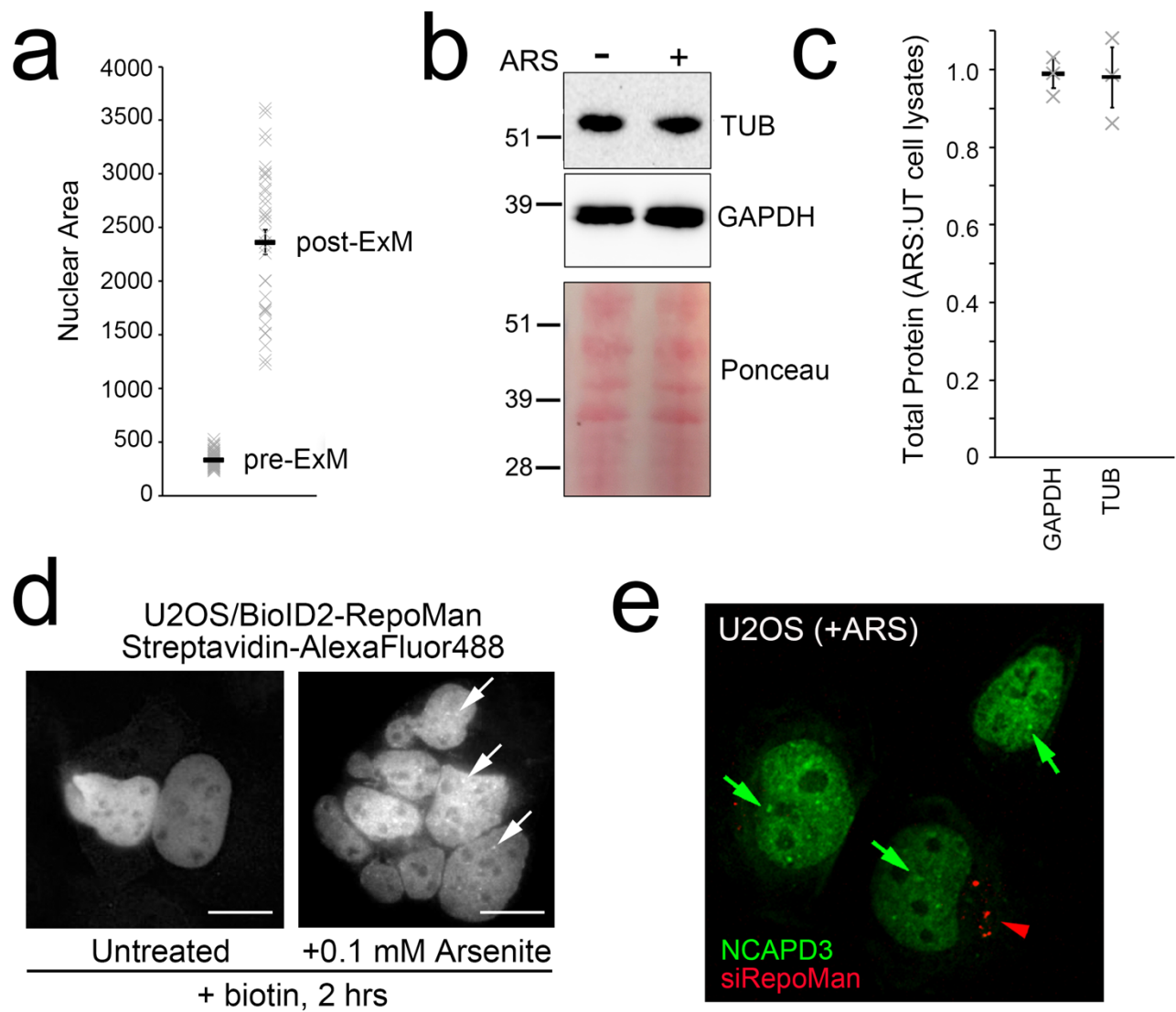


**Figure S4. Control experiments, Related to Figures 2-4.** a. Estimation of ExM expansion factor based on measurement of Hoechst 33342-stained nuclear area in pre- and post-expansion cells. Results shown here are for 92 pre-ExM and 36 post-ExM cells measured in 4 separate experiments. The average expansion factor was 7.1. b. Western blot assessing protein levels of GAPDH and alpha-tubulin (TUB) in equivalent total protein amounts (50  $\mu$ g) of U2OS whole cell lysates with and without arsenite stress (0.5 mM for 30 min). Ponceau S staining of the relevant region of the blot is shown. c. Graph showing the results of 3 independent experiments (X) and the mean  $\pm$  SE (-). For each experiment, GAPDH and TUB levels were quantified, and then normalized by the level of total stained protein in each lane (measured on a Coomassie-stained gel run in parallel). d. Coverslips included in the dishes of cells harvested for the BioID experiment (U2OS cells transduced to transiently express BioID2-RepoMan) were removed for fixation and streptavidin staining to confirm accumulation of RepoMan at arsenite-induced nucSF (arrows). e. U2OS cells stably expressing GFP-NCAPD3 were treated with Cy5-tagged siRNA targeting RepoMan for 48 hrs prior to arsenite stress. Red arrowhead indicates cell that has taken up the siRNA and green arrows indicate NCAPD3 accumulation in nuclear foci. Scale bars are 5  $\mu$ m.

## Transparent Methods

### *Plasmids and antibodies*

The pEGFP(C1)-RepoMan and pmCherry(C1)-RepoMan plasmids were previously described (Trinkle-Mulcahy et al., 2006) and are available through Addgene (plasmids #44212 and 46274). For BioID experiments, RepoMan was fused to the BioID2 tag sequence (Addgene plasmid #74223; (Kim et al., 2016)) and subcloned into the pLVX-IRES-mCherry vector (Takara Bio). Coding sequences for G3BP2 and NCAPD3 were amplified from donor constructs (obtained from ThermoFisher) and subcloned into the pEGFP-C1 expression plasmid. All cloning was confirmed by DNA sequencing (StemCore Laboratories, Ottawa Hospital Research Institute). pmCherry-PSP1 and pmCherry-TIA1 were gifts from Drs. Archa Fox and Derrick Gibbings, respectively. Antibodies that recognize HP1 $\gamma$ , H3K9me3, HSF1, Coilin, SNRPB (Y12), ADCY2 and NCAPD3 were obtained from Abcam. Alpha-tubulin and GFP antibodies were from Millipore Sigma. The G3BP antibody was from BD Biosciences, the CTCF antibody from New England Biolabs and the PML antibody from Santa Cruz Biotechnology. The TIA1 antibody was a gift from Dr. Jocelyn Côté. All HRP- and fluorophore-conjugated secondary antibodies and streptavidin were from ThermoFisher.

### *CRISPR/Cas 9 gene editing*

To knock GFP in frame upstream of Exon 1 in endogenous RepoMan, guide RNAs were designed (ThermoFisher), annealed and cloned into pSpCas9(BB)-2A-Puro (PX459) V2.0 (Ran et al., 2013) (Addgene plasmid #62988) using BbsI. The guide sequences were #1 (FWD CACCGTCGAATCACGTTTCATCTTGC; REV AAACGCAAGATGAACGTGATTCGAC), #2 (FWD CACCGATCACGTTTCATCTTGCTGGT; REV AAACACCAGCAAGATGAACGTGATC) and #4 (FWD CACCGTGAATTGGCATCCATCTAAG; REV AAACCTTAGATGGATGCCAATTCAC). A linear donor/repair template (GeneArt Strings; ThermoFisher) was designed with 800 bp left and right arms that anneal to the RepoMan gene locus near the initiating methionine flanking the GFP sequence and a linker region (5 x alanine). Silent mutations were introduced into the PAM sequences in the donor template targeted by the guide RNAs. The linear template was subcloned into pCR-Blunt (ThermoFisher), using EcoRI, for amplification. HEK293 cells were transfected with a 3:1 ratio of the circular Cas9/gRNA plasmid to the linear donor/repair template, using polyethylenimine (PEI) transfection reagent. Cells were selected by puromycin for 24 hrs and recovered in normal media. GFP-based cell sorting (uOttawa Flow Cytometry Core Facility) was used to sort 1 cell per well in a 96-well plate. Clonal lines were expanded for analysis by imaging and Western blot. RNAi-mediated knockdown of RepoMan was carried out as previously described (Trinkle-Mulcahy et al., 2006).

### *Cell culture*

The cell lines used in this study (detailed in Table S2) were all obtained from ATCC and grown in Dulbecco's modified Eagles' medium (DMEM; Wisent Bioproducts Inc.) supplemented with 10% fetal calf serum and 100 U/mL penicillin and streptomycin (Wisent Bioproducts Inc). For overnight glucose/serum starvation, cells were incubated in glucose-free DMEM (ThermoFisher). Stable cell lines were generated as previously described and maintained in media supplemented with G418 (Trinkle-Mulcahy et al., 2007). For hypoxia experiments, cells were maintained at 1% O<sub>2</sub> in a H35 HypOxyStation® hypoxia chamber (Whitley). For BioID experiments, 20  $\mu$ M biotin was added to the media for 2 hrs prior to harvesting. All drug treatments are summarized in Table S1. All chemicals were purchased from Millipore Sigma, with the exception of Olaparib (SelleckChem) and NaCl (Fisher Scientific).

### *Chromatin Immunoprecipitation*

GFP-RepoMan knock-in HEK293 cells (untreated or arsenite-stressed) were formaldehyde-fixed, scraped into PBS, pelleted and frozen in liquid N<sub>2</sub>. Native chromatin immunoprecipitation (ChIP) was performed as previously described (Brand et al., 2008), with ChIPed DNA purified by phenol-chloroform extraction and precipitated with ethanol, and GAPDH, ADCY2 and PPP2R2C DNA sequences (de Castro et al 2017) amplified with PerfeC TaSYBRGreen SuperMix (Quanta Biosciences) using a Rotor-Gene Q real-time PCR system (QIAGEN). ChIPed DNA quantity was calculated compared with a genomic DNA standard curve using Rotor-Gene Q Series Software 1.7 (QIAGEN) with R<sup>2</sup> > 0.96. Drosophila spike-in chromatin was used as an internal standard. GFP-Trap\_A resin (Chromotek) was used to capture GFP-RepoMan and Protein G Sepharose Fast Flow beads (ThermoFisher) as a negative control. Four experiments (2 x 15 cm dishes untreated vs. arsenite each) were analyzed.

#### *RT-qPCR*

Total cellular RNA was extracted from cells and reverse-transcribed, and transcripts were amplified as previously described (Chamousset et al., 2010). For qPCR, 4 µL of each cDNA reaction was analyzed in duplicate using Power Up SYBR Green Master Mix (ThermoFisher) and a CF96 Touch™ Real-Time PCR Detection System (BioRad). The comparative C<sub>T</sub> method (Schmittgen and Livak, 2008) was used to compare relative levels of mRNA in arsenite-stressed versus untreated U2OS cells, using GAPDH as an internal standard (see Fig. S4). Custom qPCR primers for GAPDH, ADCY2 and PPP2R2C were as previously described (de Castro et al 2017), with three biological replicates analyzed for each.

#### *Metabolic labeling*

Stable isotope labeling with amino acids in cell culture (SILAC) for label-based quantitative MS was carried out as previously described (Trinkle-Mulcahy et al., 2008). Briefly, cells were grown for 7-10 passages in high glucose DMEM containing either L-arginine and L-lysine (Light), or the isotopes L-arginine<sup>13</sup>C/<sup>15</sup>N and L-lysine<sup>13</sup>C/<sup>15</sup>N (Heavy). SILAC media was prepared by supplementing high glucose DMEM minus Arg/Lys/Leu/Met (AthenaES) with 10% dialyzed FBS (ThermoFisher) and the appropriate amino acids, mixing well and filtering through a 0.22 µm filter (Millipore). For the BioID experiment, Heavy isotope-encoded cells were exposed to arsenite stress. This labeling was flipped for the AP/MS experiment, with Light-encoded cells exposed to arsenite stress.

#### *Preparation of cell extracts and affinity purification*

For standard Western blots and AP/MS experiments, whole cell extracts were prepared by scraping cells into ice-cold RIPA buffer (50 mM Tris pH 7.5, 150 mM NaCl, 1% NP-40, 0.5% deoxycholate, protease inhibitors), sonicating and clearing by centrifuging at 2800g for 10 min at 4 °C. For BioID experiments, whole cell lysates were prepared in high salt (500 mM NaCl) RIPA buffer. Total protein concentrations were measured using the Pierce BCA Protein Assay Kit (ThermoFisher).

GFP-RepoMan complexes were captured from cell extracts as previously described (Prévost et al., 2013), with equal amounts of total protein extract for each condition incubated with GFP-Trap\_A beads (Chromotek) at 4°C for 1 hour. Following an initial wash with RIPA buffer, beads from the control and experimental pulldowns were combined for additional washes (to minimize variability in downstream processing) and bound proteins eluted with 1% SDS. For BioID experiments, the salt concentration in the lysates was first reduced to 250 mM by adding an equal volume of "no salt" (0 mM NaCl) RIPA buffer, and then equal amounts of total protein extract for each condition incubated with Streptavidin-agarose beads (ThermoFisher) at 4°C for 4 hours. Following an initial wash with RIPA buffer, beads from the control and experimental pulldowns were combined

for additional washes (to minimize variability in downstream processing) and bound proteins eluted with 2% SDS/30 mM biotin.

The eluted proteins were reduced and alkylated by treatment with DTT and iodoacetamide, respectively. Sample buffer was then added and the proteins resolved by electrophoresis on a NuPAGE 10% BisTris gel (Thermo Fisher). The gel was stained using SimplyBlue Safestain (Thermo Fisher) and the entire lane cut into five slices. Each slice was cut into 2 × 2 mm fragments, destained, and digested overnight at 30°C with Trypsin Gold (ThermoFisher).

#### *Mass spectrometry and data analysis*

An aliquot of each tryptic digest was analyzed by LC-MS/MS on an Orbitrap Fusion Lumos system (Thermo Scientific) coupled to a Dionex UltiMate 3000 RSLC nano HPL. The raw files were searched against the Human UniProt Database using MaxQuant software v1.5.5.1 (<http://www.maxquant.org>) (Tyanova et al., 2016) and the following criteria: peptide tolerance = 10 ppm, trypsin as the enzyme (two missed cleavages allowed), and carboxyamidomethylation of cysteine as a fixed modification. Variable modifications are oxidation of methionine and N-terminal acetylation. Heavy SILAC labels were Arg10 (R10) and Lys8 (K8). Quantitation of SILAC ratios was based on razor and unique peptides, and the minimum ratio count was 2. The peptide and protein FDR was 0.01. The BioID and AP/MS datasets (minus common environmental contaminants as per <http://maxquant.org> and proteins identified via the decoy database) are provided in Table S3.

#### *Fluorescence microscopy*

Cells seeded on No. 1.5 coverslips were fixed for 10 min at room temperature in 3.7% (wt/vol) paraformaldehyde (PFA) in CSK buffer (1mM PIPES pH 6.8, 100mM NaCl, 300mM sucrose, 3mM MgCl<sub>2</sub>, 2mM EDTA). Following a 10 min permeabilization with 1% Triton X-100 in PBS, nonspecific binding sites were blocked by incubation in PBS with 1% BSA and 0.1% Tween-20. For immunostaining, cells were incubated with the appropriate primary antibody, followed by incubation with the appropriate fluorophore-conjugated secondary antibody. Coverslips were prepared for imaging by mounting in Vectashield liquid mounting media (Vector Labs).

For live imaging, cells were cultured in 35 μm optically clear polymer-bottom μ-dishes or 4-well μ-slides (ibidi) and growth medium replaced with Phenol Red-free CO<sub>2</sub> independent medium (ThermoFisher). If desired, DNA was stained by incubating the cells for 20 min at 37°C in medium containing 0.25 μg/ml Hoechst No. 33342 (Millipore Sigma). Images were acquired using a DeltaVision CORE widefield fluorescence system fitted with a 60× NA 1.4 PlanApochromat objective (Olympus), CoolSNAP charge-coupled device (CCD) camera (Roper Scientific) and environmental chamber. The microscope was controlled and images processed by SoftWorX acquisition and deconvolution software (GE Healthcare). All images are single, deconvolved optical sections. Photobleaching experiments were carried out as previously described (Prévost et al., 2013)

#### *Expansion microscopy*

Expansion microscopy was carried out as per the X10 protocol (Truckenbrodt et al., 2019). Briefly, cells seeded on coverslips were fixed and stained as described above, followed by overnight incubation at room temperature with Acryloyl-X anchoring reagent (ThermoFisher) diluted to 0.1 mg/ml in PBS. The gelation solution was prepared by mixing 1.335g DMAA and 0.32 g sodium acrylate (both from Millipore Sigma) with 2.85 g ddH<sub>2</sub>O, vortexing and purging O<sub>2</sub> by bubbling with N<sub>2</sub> for 40 min at room temperature. A solution of 0.036 g/ml of potassium persulfate was prepared in ddH<sub>2</sub>O, 0.3 ml added to 2.7 ml of gelation solution and O<sub>2</sub> purged by bubbling with N<sub>2</sub> for 15 min on ice. Gelation chambers were prepared by sandwiching the

stained coverslip, cell side up, between two coverslips and adding spacer coverslips along the sides. 2  $\mu$ l of TEMED was added to 0.5 ml of the gel solution and vortexed, 100  $\mu$ l of gel solution was pipetted on top of the cells using a pre-chilled pipette tip and a 22 x 22 mm coverslip placed on top. Gels were placed in a humidified chamber and allowed to polymerize for 3 hours at room temperature. The gels were removed from the coverslips and placed in 35  $\mu$ m culture dishes for overnight incubation at 50°C with 8 U/ml Proteinase K (Millipore Sigma) prepared fresh in digestion buffer (50mM TRIS, 800mM Guanidine HCl, 1mM EDTA and 0.5% (v/v) Triton X-100 in ddH<sub>2</sub>O, pH 8.0). To swell the gels, they were transferred to 10 cm culture dishes and 10 ml of deionized water containing 1.7  $\mu$ g/ml Hoechst 33342 (Millipore Sigma) was added. After 10 min, this was replaced with deionized water for a further 50 min incubation. To image cells post-expansion, circular sections were punched out of the gel using the top of a P1000 pipette tip and transferred to 8-well chambered coverslips (ibidi). Multiwavelength Z-stacks were acquired using a Zeiss LSM880 confocal laser scanning microscope with a 63x/1.4 NA Plan-Apo objective in AiryScan mode (Huff, 2015). 3D Surfaces volume rendering was carried out using Imaris software (Bitplane). To calculate the expansion factor, pre- and post-expansion cells were imaged and nuclear area measured using SoftWorX (Figure S4a).

## Supplemental References

Ran, F.A., Hsu, P.D., Wright, J., Agarwala, V., Scott, D.A., Zhang, F., 2013. Genome engineering using the CRISPR-Cas9 system. *Nature Protocols* 8, 2281–2308.

Brand, M., Rampalli, S., Chaturvedi, C.-P., Dilworth, F.J., 2008. Analysis of epigenetic modifications of chromatin at specific gene loci by native chromatin immunoprecipitation of nucleosomes isolated using hydroxyapatite chromatography. *Nature Protocols* 3, 398–409.